THE JOURNAL OF PHYSICAL CHEMISTRY C

Article

Cite This: J. Phys. Chem. C 2019, 123, 4029−4034

pubs.acs.org/JPCC

Comprehensive Elucidation of Ion Transport and Its Relation to Hysteresis in Methylammonium Lead Iodide Perovskite Thin Films

Hamidreza Khassaf, Srinivas K. Yadavalli, Onkar S. Game,† Yuanyuan Zhou, Nitin P. Padture, and Angus I. Kingon*

School of Engineering, Brown University, Providence, Rhode Island 02912, United States

ABSTRACT: The "dark" current−voltage (I−V) response of $CH_3NH_3PbI_3$ organic−inorganic halide perovskite (OIHP) thin films is studied as a function of temperature, voltage, and scan rate to investigate the nature of the I−V hysteresis. This is to address the apparent discrepancy observed in characteristics of the I−V hysteresis. Depending on the measurement conditions, two complementary mechanisms appear to control the I−V behavior. First, ionic species contribute to the conduction, and because of their slow-moving nature, a slower scan rate gives ions enough time to take part in conduction (i.e., below a relaxation frequency). Second, migration of ionic species to the interface(s) modulates the Schottky junction and, consequently, the electronic transport across the interfaces. Therefore, a slower scan rate results in more charge accumulation at the interface, which leads to a decrease in the leakage current. These findings provide an explanation that resolves the ongoing debate regarding the characteristics of the I−V hysteresis in solar cells based on OIHPs.

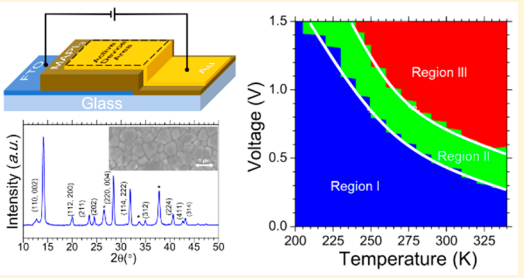

INTRODUCTION

There has been growing interest in studying the fundamental properties of organic−inorganic halide perovskites (OIHPs) in recent years.[1,2] The fact that this class of materials exhibit exceptional electrical and optical properties such as low trap densities,[2] strong absorption,[3] and long carrier diffusion lengths,[2] along with their low-cost solution processability and low processing temperature, makes them excellent candidates for perovskite solar cells (PSCs) and other optoelectronic devices.[4−6] While there has been an abundance of research in this area, debate still exists around the fundamental characteristics of OIHPs such as dielectric and ferroelectric behavior;[7,8] degradation induced by electric field, light, and temperature;[9,10] and the nature of charge transport and current−voltage (I−V) hysteresis.[11,12] In particular, several papers have been published on the characterization of the hysteretic behavior of "dark" (and "photo") current in OIHPs, where a combination of several factors can play a role in the observed hysteresis in OIPs. While there is extensive debate on whether or not methylammonium lead iodide ($CH_3NH_3PbI_3$ or $MAPbI_3$) as a prototype for OIHP exhibits ferroelectric (FE) behavior,[13,14] Chen et al.[15] suggest a correlation between field-induced FE polarization of $MAPbI_3$ and the enhancement of hysteresis. Shao et al.[16] have attributed the I−V hysteresis to the presence of large densities of charge traps at the interface and also at grain boundaries. On the other hand, there are studies that argue plausibly that, first, ferroelectricity cannot explain the I−V hysteresis because there is an upper limit of around 1 $\mu C \cdot cm^{-2}$ for intrinsic frequency−dependent polarization.[14] Second, due to relatively high electronic mobility (it takes nanoseconds for electrons to reach the interface), it is unlikely that charge traps play a singular or dominating role in the observed I−V hysteresis.[17] Therefore, the main argument revolves around which types of (relatively) slow-moving ions and defects contribute to the charge transport in OIHPs resulting in the I−V hysteresis.[18−22]

Several studies have suggested that one of the dominant charge-transport mechanisms in $MAPbI_3$ is through ion migration.[23−28] They often report a single value for activation energy with magnitudes that vary widely, in the range 0.1−0.6 eV. This further adds to the uncertainty regarding the nature of this migrating species and also fails to notice the possibility that carrier transport may be obscured by vacancy-mediated migration of ions that differ in activation energy. Our previous study on $MAPbI_3$ thin films using pulse discharge and direction/scan rate and temperature-dependent I−V demonstrated that,[18] depending on the measurement conditions such as temperature, voltage, applied-voltage history, and scan rate, electronic transport varies significantly.[18] We presented a clear indication that a mechanism that involves migration and accumulation of ions at the interface moderates carrier transport in $MAPbI_3$. We were then able to capture two distinctive thermally activated processes, with activation energies of E_a = 0.41 ± 0.02 and 0.1 ± 0.001 eV that we assigned to electromigration of MA^+ cations and I^- anions, respectively. Accumulation of these two ionic species then contributes significantly to the modification of interfacial electronic properties. While there is now a relatively clear

Received: November 21, 2018
Revised: January 20, 2019
Published: January 22, 2019

DOI: 10.1021/acs.jpcc.8b11285
J. Phys. Chem. C 2019, 123, 4029−4034

picture of how various ionic species contribute to charge transport in $MAPbI_3$, there are still unaddressed questions regarding the effect of scan rate and its effect on the hysteretic behavior in OIHPs. Although there is agreement that the nature of the $I-V$ curve, including current magnitude and hysteresis, shows a strong dependency on the scan rate, there appears to be certain discrepancies in the observed behavior. On one hand, some research groups observe that the magnitude of current increases with a decrease in the scan rate but the apparent $I-V$ hysteresis decreases.[29,30] This behavior is attributed to the hypothesis that, since the $I-V$ hysteresis behavior is predominantly due to ion migration ("migration-dominated" behavior), the leakage current increases if the voltage is applied to the device long enough so that the slow-moving ions can partake more in the flow of the current. On the other hand, some groups report that, while the hysteresis diminishes with an increase in the scan rate, the magnitude of the current increases for faster scan rates.[31,32] The origin of this behavior is the subject of debate. Seol et al.[31] suggest that the contribution of the transient current of polarization switching adds to the leakage current for fast scanning. However, a plausible counter argument questions this explanation considering that the upper limit of intrinsic frequency-dependent polarization is around 1 $\mu C \cdot cm^{-2}$.[14] On the other hand, Guan et al.[32] propose that an interface-modulation mechanism is responsible for this behavior where faster voltage scan rates cause less ionic accumulation at the interface, and this leads to a smaller Schottky barrier. As a result, current flow is easier at higher scan rates ("accumulation-dominated" behavior). Here we continue our previously reported work by carrying out temperature- and rate-dependent $I-V$ measurements in "dark" conditions with the aim to extend our understanding of the nature of ion movements in OIHPs. We particularly perform our characterization on a metal−semiconductor−metal (M−S−M) configuration and under dark conditions to avoid photogenerated carriers in order to isolate the ionic−electronic transport. As such, the simple M−S−M allows us to study the intrinsic behavior of $MAPI_3$ without dealing with complex device architecture with electron- and hole-selective layers. We suggest a mechanism which reconciles both aforementioned observations in such a way that, depending on the measurement conditions, both migration- and accumulation-dominated behaviors are convincingly justified.

RESULTS AND DISCUSSION

In order to isolate the charge-transport behavior in $MAPbI_3$, we fabricated devices with a typical metal−semiconductor−metal (M−S−M) capacitor-like configuration. These devices consist of $MAPbI_3$ films asymmetrically sandwiched in between fluorine-doped tin oxide (FTO) and Au as electrodes. The work function of both electrodes in such a device is close to 5 eV.[33] We cut 15 mm × 15 mm squares of FTO substrates (Hartford Glass, USA) with a sheet resistance of 8 Ω/sq. and then etched them using zinc dust and dilute aqueous hydrochloric acid. As for the cleaning process, substrates were washed using soap and deionized water and subsequently with absolute ethanol. In a final stage, they underwent ozone treatment for approximately 30 min before film deposition. The "solvent-engineering" solution-based method[34] was used to deposit the $MAPbI_3$ films onto the FTO substrates as follows: 40 wt % $MAPbI_3$ solution was prepared by dissolving PbI_2 (Sigma-Aldrich, USA; 99.9995%) and MAI (Great-Cell Solar, Australia) in a stoichiometric (1:1) ratio in *N*,*N*-dimethylformamide (DMF) solvent. This precursor solution was spin-coated on cleaned FTO substrate at 2000 rpm for 30 s followed by chlorobenzene dripping while spinning. The films were then heated at 130 °C for 10 min. The final $MAPbI_3$ films had thicknesses of ∼300 nm, as determined by a step profilometer. In order to prevent degradation in the process of making the OHIP, all steps of film preparation were performed inside a N_2-filled glovebox. As-deposited $MAPbI_3$ thin films were characterized by X-ray diffraction (XRD) (D8 Discover, Bruker, Germany) using Cu Kα radiation and by scanning electron microscopy (SEM; LEO, Zeiss, Germany) for crystallographic and microstructural characterization, respectively. Au contacts of ∼120 nm thick were deposited in the thermal evaporation chamber under a base pressure of $\sim 10^{-7}$ Torr.

As can be seen in Figure 1, the active area of the fabricated device lies where the geometric area of gold, $MAPbI_3$, and

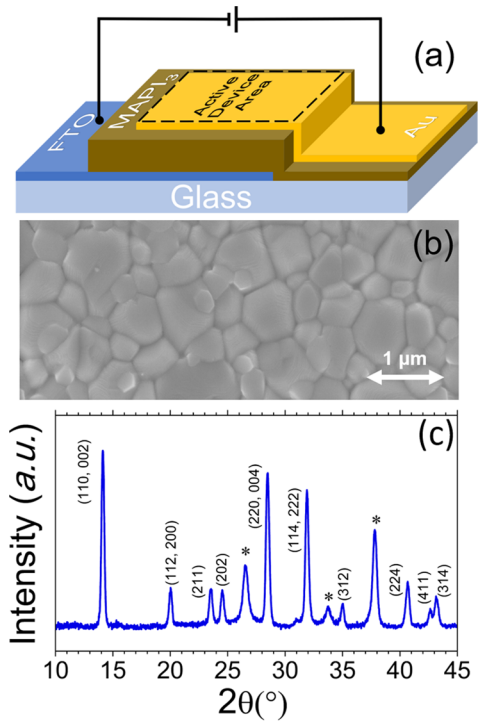

Figure 1. (a) Schematic illustration of the device with FTO−$MAPbI_3$−Au configuration. The "high" and "low" of the sourcemeter were connected to the Au and FTO electrodes, respectively. Dashed lines indicate the active device area. (b) Top-view SEM of as-prepared $MAPbI_3$ thin film. (c) Indexed XRD pattern of the $MAPbI_3$ film, where ∗ indicates reflections from the underlying FTO.

FTO overlap. A schematic diagram of the device is illustrated in Figure 1a. In order to perform temperature-dependent measurements, the device was placed in a cryostat chamber (VPF-100, Janis), where it was kept under a constant vacuum (pressure of $\sim 10^{-3}$ Torr) throughout the measurements. A temperature controller (335, Lakeshore) was used inside the cryostat to stabilize the device at the desired temperature. Electrical measurements were performed using a sourcemeter (2635A, Keithley). As a reference, the Au top electrode was always connected to the "high" leads and the FTO bottom electrode to the "low" leads of the sourcemeter. Figure 1b shows a top-view SEM micrograph of the $MAPbI_3$ thin film,

DOI: 10.1021/acs.jpcc.8b11285
J. Phys. Chem. C 2019, 123, 4029−4034

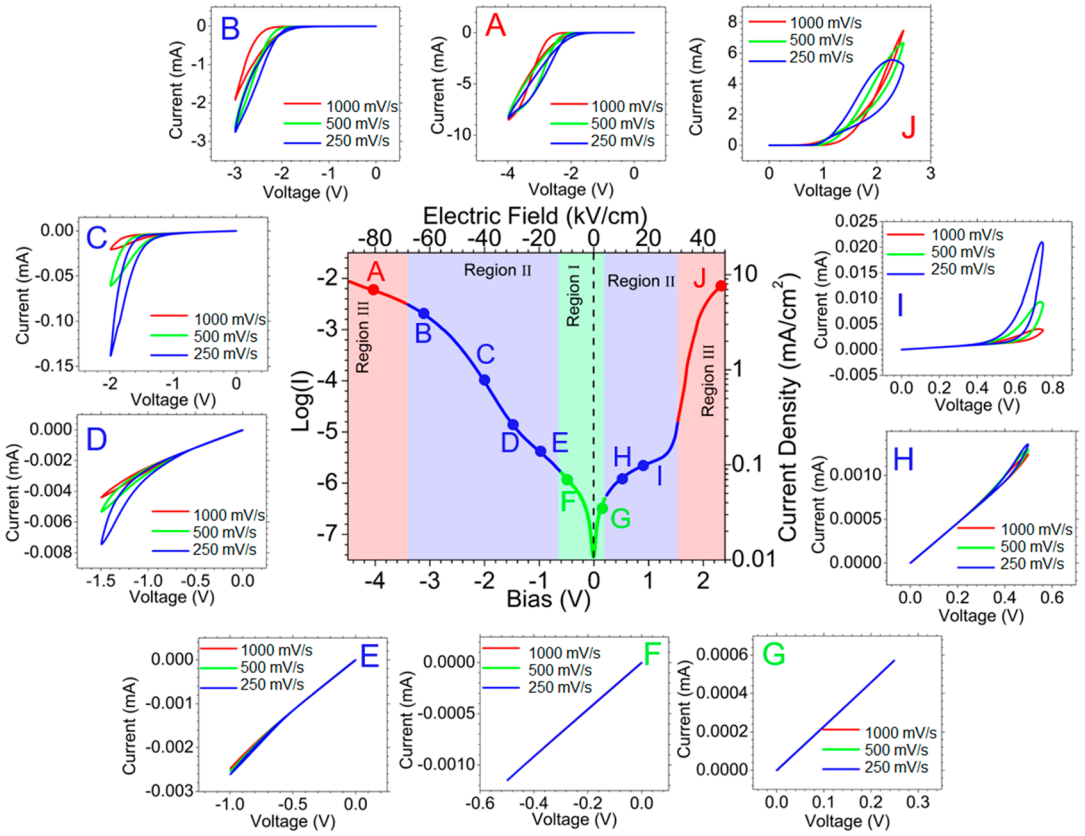

Figure 2. $I-V$ plot of $MAPbI_3$ film under negative and positive biases showing asymmetry with three types of behavior on each side. Region I shows Ohmic response, whereas regions II and III exhibit "migration-dominated" and "accumulation-dominated" behaviors, respectively. Plots A–G show how the scan rate impacts the leakage current depending on the region to which bias strength belongs.

confirming a smooth, dense, and uniform surface. The average grain size is estimated to be ∼600 nm. Figure 1c shows an indexed XRD pattern of the $MAPbI_3$ film confirming the tetragonal phase (space group $I4/mcm$).

Figure 2 presents the $I-V$ behavior of $MAPbI_3$ film at T = 300 K. As can be seen, there is a high degree of asymmetry evident in the curve from negative to positive biases. For example, the leakage current at $V = +2$ V is $I = 2.5 \times 10^{-3}$ A, whereas, for $V = -2$ V, it is $I = 9.3 \times 10^{-5}$ A. A high degree of asymmetry in this level (nearly 2 orders of magnitude at $V = \pm 2$ V) is unlikely to be due to the small difference in work functions of Au and FTO. In fact, recent studies on OIHP material systems with similar configurations suggest that the asymmetry can be attributed to a difference in the interfacial electronic structure at the two interfaces.[35] Therefore, one can postulate that the presence of such an asymmetry may be originating from different levels of accumulation of defects at the interfaces. In the case of OIHPs, since the formation energies of vacancy defects are particularly low, microstructural imperfections at the interfaces such as grain boundaries and free surfaces make interfaces desirable for defects to accumulate. It has been reported that OIHP single crystals have a higher vacancy concentration on the surface compared to the bulk.[36,37] Therefore, in our case, it is reasonable to assume that charge accumulation at the Au–$MAPbI_3$ interface is significantly different from that at the buried FTO–$MAPbI_3$ interface.

Plots A–G in Figure 2 exhibit how the scan rate impacts the leakage current depending on the region to which bias strength belongs. For region I (F and G), the $I-V$ curve exhibits Ohmic behavior, where the current increases linearly with voltage and there is no apparent hysteresis observed. Also, changing the scan rate has no effect on the observed current. In the case of $I-V$ curves in region II (B, C, D, E, H, and I, accumulation-dominated behavior), hysteresis is evident where lowering the scan rate leads to a higher current. This behavior is similar to the reported migration-dominated behavior described earlier.[29,30] Here, as various ionic species contribute to conduction and because of their slow-moving nature, slower scan rates give ions enough time to take part in conduction, resulting in an increase in the leakage current. Also, the reverse-scan current, i.e., the current measured by reducing the voltage toward zero, is larger in magnitude than that for the forward-scan current. It is due to the fact that there are more already activated ion species available from the forward bias when the reverse bias is applied. These ion species will add to the ionic contribution and result in a relatively higher leakage current. Finally, in region III (A and J, charge accumulation), while the hysteresis is still present, its characteristics change, and increasing the scan rate results in a higher current. The observed behavior here matches with what has been reported as accumulation-dominated behavior.[31,32] In this case, Schottky-junction height modulation originating from migration of ion species to the interface dictates the magnitude of current by setting a barrier height that controls the current flow. Here, accumulation of ionic species increases the barrier height. Therefore, slower scan rates, which result in more accumulation at the interface, lead to a decrease in leakage current. Another observed behavior that corroborates the proposed mechanism is that the reverse-scan current is smaller

DOI: 10.1021/acs.jpcc.8b11285
J. Phys. Chem. C 2019, 123, 4029–4034

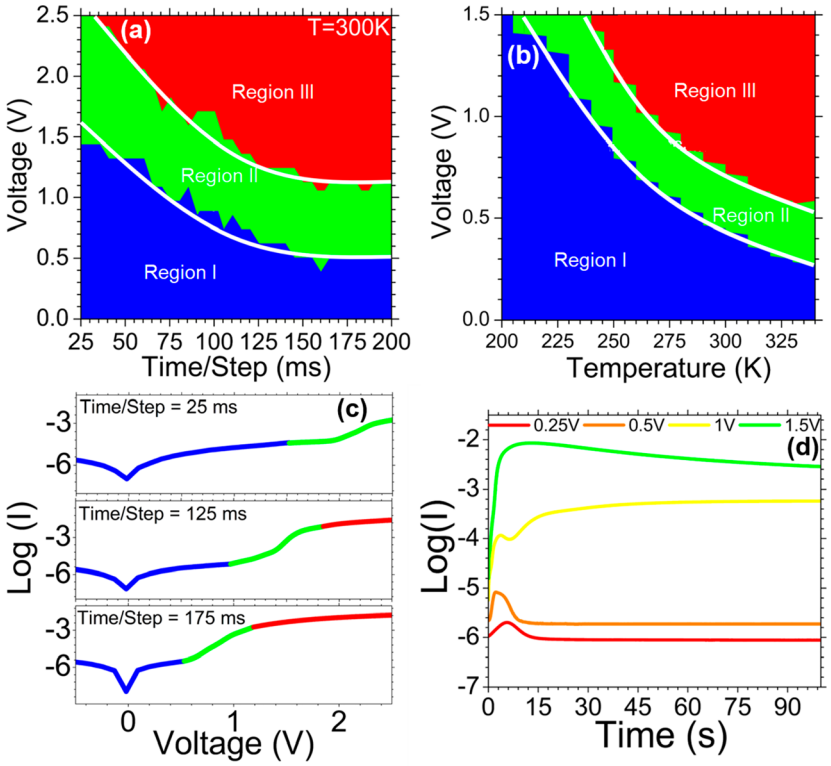

Figure 3. (a) Bias/scan rate (at 300 K) and (b) bias/temperature (at 250 ms/step) maps showing the stability of the various regions. (c) Three representative $I-V$ curves at 300 K. (d) Leakage current behavior of $MAPbI_3$ film over time under continuous applied biases from 0.25 to 1.5 V at 300 K. In all cases, the device was first conditioned by a reverse applied voltage of −1.5 V for 20 s. For biases less than 1 V, there is a peak before 10 s is passed, and after that, the leakage stabilizes at a value lower than the maximum. For biases of 1 V, the stabilized magnitude of leakage is larger than the relative maximum. In the case of V = 1.5 V, the magnitude of leakage starts to decrease over time due to accumulation of charges at the interface.

in magnitude compared to the forward-scan current. This can be attributed to the fact that, during forward bias, there will be a certain level of charge accumulation at the interface. This will cause a barrier height increase, leading to a smaller leakage current in reverse bias.

Therefore, as can be seen in Figure 2, depending upon the level of activity of the ionic species in the OIHP, the hysteretic dynamics can vary from no hysteresis (Ohmic region, region I), to migration-dominated (region II), to accumulation-dominated (region III) behaviors. The type of OIHP and the measurement conditions, such as temperature, voltage, and scan rate, will dictate the nature of the hysteresis. This proposed classification can then convincingly explain and reconcile both seemingly divergent observations of characteristics of the $I-V$ hysteresis.

Furthermore, in order to independently determine the effect of each parameter on the type of observed hysteresis, we performed measurements at various temperatures, voltages, and scan rates.

Figure 3a presents a map of the stability of the various regions as a function of scan rate at 300 K for $MAPbI_3$. As can be seen, a shorter time per step (faster scan rates) and lower bias tend to stabilize the Ohmic region, whereas a relatively longer time per step (slower scan rates) and higher bias first result in the stabilization of the migration-dominated behavior and eventually give rise to the accumulation-dominated behavior, where charge accumulation at the interface dictates the characteristics of the hysteresis. Figure 3b exhibits a similar region-stability map as a function of temperature at a scan rate of 250 ms/step. Here, comparable behavior is observed, where lower temperature reduces the mobility of ionic species and stabilizes the Ohmic region. On the other hand, increasing the temperature results in the activation of ionic species, and together with relatively high bias, the hysteresis characteristics initially are dictated by migration-dominated behavior, and the further intensification of the parameters leads to Schottky barrier modulation and attendant accumulation-dominated behavior. Figure 3c presents $I-V$ curves of three representative scan step lengths (25, 125, and 175 ms/step). For a scan pace of 25 ms/step, regions I and II are observed. As the scan step length shifts to higher values (slower scan rates), contribution of ionic species becomes more pronounced, and as a result, the two types of hysteresis are observed at relatively smaller biases. Figure 3d shows the leakage current behavior of $MAPbI_3$ film over time and under continuous applied biases ranging from 0.25 to 1.5 V. It should be noted that, in all cases, the device underwent a reverse applied voltage of −1.5 V for 20 s. For biases of <1 V, there is a peak before 10 s is passed, and after that the leakage stabilizes at a value lower than the maximum. For a bias of 1 V, the stabilized magnitude of leakage is larger than the relative maximum. In the case of V = 1.5 V, the magnitude of leakage starts to decrease over time due to the accumulation of charges at the interface. This categorization of $I-V$ characteristics clearly signifies the crucial role of charged species which can migrate toward, and accumulate at, the electrode interfaces and are responsible for modification of the electronic character of the device. Therefore, it is important to note that, as this electromigration is tightly related to and

DOI: 10.1021/acs.jpcc.8b11285
J. Phys. Chem. C 2019, 123, 4029−4034

impacted by factors such as film quality, chemical composition, and interface configuration, one can expect electrical behavioral changes as a result of a change in any of these configurational characteristics. Nevertheless, our work shows that in order to control hysteresis it is necessary to address ionic transport. Methods to achieve this are beyond the scope of this paper but are being addressed in current research.

CONCLUSIONS

In summary, here we provide a framework for a comprehensive study of various types of hysteresis behaviors observed in OIHPs. It addresses the debate around the seemingly contradictory observations made by different research groups and presents an explanation that reconciles the different interpretations. It is suggested that the hysteretic effects, and their qualitative characteristics, are a consequence of the measurement conditions and are an intrinsic property of the OIHP rather than being related to fabrication methods or other elements of the PSC. Depending on the measurement condition and protocol, slow-moving ionic species determine the conduction mechanism and hysteretic dynamics. As many reports have suggested, dynamic hysteresis is the consequence of PSC degradation.[38−40] Therefore, in order to develop commercially viable PCSs, understanding the hysteretic phenomenon in OIHPs is a crucially important part of a comprehensive knowledge about the PSCs. The observed scan-rate-dependent hysteretic behavior in this work suggests that the origin of hysteresis in perovskite solar cells is most likely to be intrinsic to the perovskite layer rather than differential charge extraction rates of electron- and hole-transport layers under illumination. Therefore, in order to mitigate the hysteretic effect, it is reasonable to focus on ways to control ionic species that are available in the medium and could generate internal fields, and also impact the Schottky barrier at the interface.

AUTHOR INFORMATION

Corresponding Author

*E-mail: angus_kingon@brown.edu.

ORCID

Hamidreza Khassaf: 0000-0002-9869-0745

Onkar S. Game: 0000-0002-5573-3602

Nitin P. Padture: 0000-0001-6622-8559

Angus I. Kingon: 0000-0002-0767-2892

Present Address

†O.S.G.: Department of Physics and Astronomy, University of Sheffield, Sheffield S3 7RH, U.K.

Notes

The authors declare no competing financial interest.

ACKNOWLEDGMENTS

This research is supported by the National Science Foundation (Grant No. OIA-1538893).

REFERENCES

(1) Zhang, W.; Eperon, G. E.; Snaith, H. J. Metal halide perovskites for energy applications. *Nature Energy* **2016**, *1* (6), 16048.

(2) Stranks, S. D.; Snaith, H. J. Metal-halide perovskites for photovoltaic and light-emitting devices. *Nat. Nanotechnol.* **2015**, *10* (5), 391.

(3) De Wolf, S.; Holovsky, J.; Moon, S.-J.; Löper, P.; Niesen, B.; Ledinsky, M.; Haug, F.-J.; Yum, J.-H.; Ballif, C. Organometallic halide perovskites: sharp optical absorption edge and its relation to photovoltaic performance. *J. Phys. Chem. Lett.* **2014**, *5* (6), 1035−1039.

(4) Kojima, A.; Teshima, K.; Shirai, Y.; Miyasaka, T. Organometal halide perovskites as visible-light sensitizers for photovoltaic cells. *J. Am. Chem. Soc.* **2009**, *131* (17), 6050−6051.

(5) Kim, H.-S.; Lee, C.-R.; Im, J.-H.; Lee, K.-B.; Moehl, T.; Marchioro, A.; Moon, S.-J.; Humphry-Baker, R.; Yum, J.-H.; Moser, J. E. Lead iodide perovskite sensitized all-solid-state submicron thin film mesoscopic solar cell with efficiency exceeding 9%. *Sci. Rep.* **2012**, *2*, 591.

(6) Lee, M. M.; Teuscher, J.; Miyasaka, T.; Murakami, T. N.; Snaith, H. J. Efficient hybrid solar cells based on meso-superstructured organometal halide perovskites. *Science* **2012**, *338*, 643.

(7) Kutes, Y.; Ye, L.; Zhou, Y.; Pang, S.; Huey, B. D.; Padture, N. P. Direct observation of ferroelectric domains in solution-processed $CH_3NH_3PbI_3$ perovskite thin films. *J. Phys. Chem. Lett.* **2014**, *5* (19), 3335−3339.

(8) Juarez-Perez, E. J.; Sanchez, R. S.; Badia, L.; Garcia-Belmonte, G.; Kang, Y. S.; Mora-Sero, I.; Bisquert, J. Photoinduced giant dielectric constant in lead halide perovskite solar cells. *J. Phys. Chem. Lett.* **2014**, *5* (13), 2390−2394.

(9) Hoke, E. T.; Slotcavage, D. J.; Dohner, E. R.; Bowring, A. R.; Karunadasa, H. I.; McGehee, M. D. Reversible photo-induced trap formation in mixed-halide hybrid perovskites for photovoltaics. *Chemical Science* **2015**, *6* (1), 613−617.

(10) deQuilettes, D. W.; Burlakov, V. M.; Graham, D. J.; Leijtens, T.; Osherov, A.; Bulović, V.; Snaith, H. J.; Ginger, D. S.; Stranks, S. D. Photo-induced halide redistribution in organic−inorganic perovskite films. *Nat. Commun.* **2016**, *7*, 11683.

(11) Brenner, T. M.; Egger, D. A.; Kronik, L.; Hodes, G.; Cahen, D. Hybrid organic—inorganic perovskites: low-cost semiconductors with intriguing charge-transport properties. *Nature Reviews Materials* **2016**, *1*, 15007.

(12) Snaith, H. J.; Abate, A.; Ball, J. M.; Eperon, G. E.; Leijtens, T.; Noel, N. K.; Stranks, S. D.; Wang, J. T.-W.; Wojciechowski, K.; Zhang, W. Anomalous hysteresis in perovskite solar cells. *J. Phys. Chem. Lett.* **2014**, *5* (9), 1511−1515.

(13) Fan, Z.; Xiao, J.; Sun, K.; Chen, L.; Hu, Y.; Ouyang, J.; Ong, K. P.; Zeng, K.; Wang, J. Ferroelectricity of $CH_3NH_3PbI_3$ perovskite. *J. Phys. Chem. Lett.* **2015**, *6* (7), 1155−1161.

(14) Beilsten-Edmands, J.; Eperon, G.; Johnson, R.; Snaith, H.; Radaelli, P. Non-ferroelectric nature of the conductance hysteresis in $CH_3NH_3PbI_3$ perovskite-based photovoltaic devices. *Appl. Phys. Lett.* **2015**, *106* (17), 173502.

(15) Chen, H.-W.; Sakai, N.; Ikegami, M.; Miyasaka, T. Emergence of hysteresis and transient ferroelectric response in organo-lead halide perovskite solar cells. *J. Phys. Chem. Lett.* **2015**, *6* (1), 164−169.

(16) Shao, Y.; Xiao, Z.; Bi, C.; Yuan, Y.; Huang, J. Origin and elimination of photocurrent hysteresis by fullerene passivation in $CH_3NH_3PbI_3$ planar heterojunction solar cells. *Nat. Commun.* **2014**, *5*, 5784.

(17) Richardson, G.; O'Kane, S. E.; Niemann, R. G.; Peltola, T. A.; Foster, J. M.; Cameron, P. J.; Walker, A. B. Can slow-moving ions explain hysteresis in the current−voltage curves of perovskite solar cells? *Energy Environ. Sci.* **2016**, *9* (4), 1476−1485.

(18) Game, O. S.; Buchsbaum, G. J.; Zhou, Y.; Padture, N. P.; Kingon, A. I. Ions Matter: Description of the Anomalous Electronic Behavior in Methylammonium Lead Halide Perovskite Devices. *Adv. Funct. Mater.* **2017**, *27* (16), 1606584.

(19) Tress, W.; Marinova, N.; Moehl, T.; Zakeeruddin, S. M.; Nazeeruddin, M. K.; Grätzel, M. Understanding the rate-dependent J−V hysteresis, slow time component, and aging in $CH_3NH_3PbI_3$ perovskite solar cells: the role of a compensated electric field. *Energy Environ. Sci.* **2015**, *8* (3), 995−1004.

(20) Bryant, D.; Wheeler, S.; O'Regan, B. C.; Watson, T.; Barnes, P. R.; Worsley, D.; Durrant, J. Observable hysteresis at low temperature in "hysteresis free" organic−inorganic lead halide perovskite solar cells. *J. Phys. Chem. Lett.* **2015**, *6* (16), 3190−3194.

DOI: 10.1021/acs.jpcc.8b11285
J. Phys. Chem. C 2019, 123, 4029−4034

(21) Heo, J. H.; You, M. S.; Chang, M. H.; Yin, W.; Ahn, T. K.; Lee, S.-J.; Sung, S.-J.; Kim, D. H.; Im, S. H. Hysteresis-less mesoscopic $CH_3NH_3PbI_3$ perovskite hybrid solar cells by introduction of Li-treated TiO_2 electrode. *Nano Energy* **2015**, *15*, 530−539.
(22) Xu, J.; Buin, A.; Ip, A. H.; Li, W.; Voznyy, O.; Comin, R.; Yuan, M.; Jeon, S.; Ning, Z.; McDowell, J. J. Perovskite−fullerene hybrid materials suppress hysteresis in planar diodes. *Nat. Commun.* **2015**, *6*, 7081.
(23) Yuan, Y.; Huang, J. Ion migration in organometal trihalide perovskite and its impact on photovoltaic efficiency and stability. *Acc. Chem. Res.* **2016**, *49* (2), 286−293.
(24) Eames, C.; Frost, J. M.; Barnes, P. R.; O'regan, B. C.; Walsh, A.; Islam, M. S. Ionic transport in hybrid lead iodide perovskite solar cells. *Nat. Commun.* **2015**, *6*, 7497.
(25) Li, Z.; Xiao, C.; Yang, Y.; Harvey, S. P.; Kim, D. H.; Christians, J. A.; Yang, M.; Schulz, P.; Nanayakkara, S. U.; Jiang, C.-S. Extrinsic ion migration in perovskite solar cells. *Energy Environ. Sci.* **2017**, *10* (5), 1234−1242.
(26) Yang, T. Y.; Gregori, G.; Pellet, N.; Grätzel, M.; Maier, J. The significance of ion conduction in a hybrid organic−inorganic lead-iodide-based perovskite photosensitizer. *Angew. Chem.* **2015**, *127* (27), 8016−8021.
(27) Kim, G. Y.; Senocrate, A.; Yang, T.-Y.; Gregori, G.; Grätzel, M.; Maier, J. Large tunable photoeffect on ion conduction in halide perovskites and implications for photodecomposition. *Nat. Mater.* **2018**, *17* (5), 445.
(28) Zhao, Y.-C.; Zhou, W.-K.; Zhou, X.; Liu, K.-H.; Yu, D.-P.; Zhao, Q. Quantification of light-enhanced ionic transport in lead iodide perovskite thin films and its solar cell applications. *Light: Sci. Appl.* **2016**, *6* (5), No. e16243.
(29) Unger, E.; Hoke, E.; Bailie, C.; Nguyen, W.; Bowring, A.; Heumüller, T.; Christoforo, M.; McGehee, M. Hysteresis and transient behavior in current−voltage measurements of hybrid-perovskite absorber solar cells. *Energy Environ. Sci.* **2014**, *7* (11), 3690−3698.
(30) Meng, L.; You, J.; Guo, T.-F.; Yang, Y. Recent advances in the inverted planar structure of perovskite solar cells. *Acc. Chem. Res.* **2016**, *49* (1), 155−165.
(31) Seol, D.; Jeong, A.; Han, M. H.; Seo, S.; Yoo, T. S.; Choi, W. S.; Jung, H. S.; Shin, H.; Kim, Y. Origin of Hysteresis in $CH_3NH_3PbI_3$ Perovskite Thin Films. *Adv. Funct. Mater.* **2017**, *27* (37), 1701924.
(32) Guan, X.; Hu, W.; Haque, M. A.; Wei, N.; Liu, Z.; Chen, A.; Wu, T. Light-Responsive Ion-Redistribution-Induced Resistive Switching in Hybrid Perovskite Schottky Junctions. *Adv. Funct. Mater.* **2018**, *28* (3), 1704665.
(33) Helander, M. G.; Greiner, M.; Wang, Z.; Tang, W.; Lu, Z. Work function of fluorine doped tin oxide. *J. Vac. Sci. Technol., A* **2011**, *29* (1), 011019.
(34) Jeon, N. J.; Noh, J. H.; Kim, Y. C.; Yang, W. S.; Ryu, S.; Seok, S. I. Solvent engineering for high-performance inorganic−organic hybrid perovskite solar cells. *Nat. Mater.* **2014**, *13* (9), 897.
(35) Xiao, Z.; Huang, J. Energy-Efficient Hybrid Perovskite Memristors and Synaptic Devices. *Advanced Electronic Materials* **2016**, *2* (7), 1600100.
(36) Komesu, T.; Huang, X.; Paudel, T. R.; Losovyj, Y. B.; Zhang, X.; Schwier, E. F.; Kojima, Y.; Zheng, M.; Iwasawa, H.; Shimada, K. Surface Electronic Structure of Hybrid Organo Lead Bromide Perovskite Single Crystals. *J. Phys. Chem. C* **2016**, *120* (38), 21710−21715.
(37) Wu, B.; Nguyen, H. T.; Ku, Z.; Han, G.; Giovanni, D.; Mathews, N.; Fan, H. J.; Sum, T. C. Discerning the surface and bulk recombination kinetics of organic−inorganic halide perovskite single crystals. *Adv. Energy Mater.* **2016**, *6* (14), 1600551.
(38) Calado, P.; Telford, A. M.; Bryant, D.; Li, X.; Nelson, J.; O'Regan, B. C.; Barnes, P. R. Evidence for ion migration in hybrid perovskite solar cells with minimal hysteresis. *Nat. Commun.* **2016**, *7*, 13831.
(39) Ginting, R. T.; Jeon, M.-K.; Lee, K.-J.; Jin, W.-Y.; Kim, T.-W.; Kang, J.-W. Degradation mechanism of planar-perovskite solar cells: correlating evolution of iodine distribution and photocurrent hysteresis. *J. Mater. Chem. A* **2017**, *5* (9), 4527−4534.
(40) Besleaga, C.; Abramiuc, L. E.; Stancu, V.; Tomulescu, A. G.; Sima, M.; Trinca, L.; Plugaru, N.; Pintilie, L.; Nemnes, G. A.; Iliescu, M. Iodine migration and degradation of perovskite solar cells enhanced by metallic electrodes. *J. Phys. Chem. Lett.* **2016**, *7* (24), 5168−5175.

DOI: 10.1021/acs.jpcc.8b11285
J. Phys. Chem. C 2019, 123, 4029−4034